Experiment overview: LHCb

Thomas Boettcher[1,2,*]

[1]Indiana University, Bloomington, IN 47405, USA
[2]Los Alamos National Laboratory, Los Alamos, NM 87544, USA

Abstract. The LHCb experiment features unique detector capabilities, forward acceptance, and a fixed-target system that enable a broad heavy-ion physics program. These features provide opportunities to study unexplored kinematics, collisions systems, and heavy-flavor probes. As a result, LHCb can help disentangle the effects of hadronization, the high-temperature medium, and the initial state configuration of heavy-ion collisions. These proceedings discuss an overview of results presented by the LHCb collaboration at Quark Matter 2025 in Frankfurt, Germany.

1 Introduction

The LHCb detector is a single-arm forward spectrometer at the Large Hadron Collider [1]. LHCb serves as a general-purpose detector at forward rapidity with precise vertex reconstruction and particle identification capabilities. In addition, LHCb features a gas injection system called SMOG, which allows LHCb to function as a fixed-target experiment. As a result, LHCb covers a unique kinematic regime, having access to forward rapidity in collider mode and central rapidity in fixed-target mode. Furthermore, LHCb can probe a wide range of center-of-mass energies, from $\sqrt{s_{(\mathrm{NN})}} \sim 100$ GeV in fixed-target model to $\sqrt{s} = 13.6$ TeV in collider mode. SMOG also allows LHCb to study a wide variety of collision systems, from fixed-target $p\mathrm{H}_2$ to PbAr. Excellent vertexing and particle ID (PID) capabilities LHCb to access unexplored heavy-flavor probes in these collision systems. In combination, these qualities give LHCb multiple ways to vary the inital state configuration, the properties of the high-temperature medium created, and the hadronization environment of heavy-ion collisions. As a result, LHCb can provide unique insight into the physical origins of phenomena observed in high-energy nuclear collisions.

2 Small systems

One of the primary goals of heavy-ion physics over the last decade has been understanding the origin of QGP-like effects in small collision systems such as pp and pPb. Collective flow, which was originally thought to be a signature of QGP production, has been observed in pPb and pp collisions [2–5]. LHCb has now for the first time measured flow coefficients as a function of event multiplicity in pPb in both the proton- and lead-going directions [6]. The measured v_2 (elliptic flow) and v_3 (triangular flow) are shown in Fig. 1. The proton- and lead-going results show similar behavior as a function of charged-particle multiplicity

*e-mail: t.boettcher@cern.ch

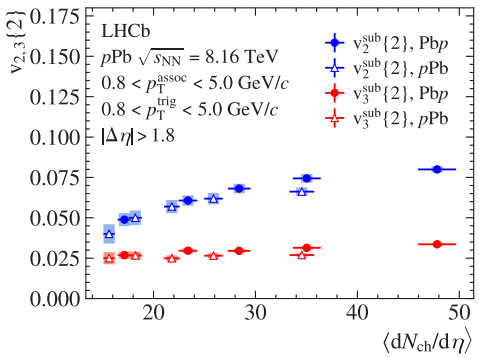

Figure 1. Flow coefficients v_2 and v_3 measured as a function of event multiplicity in pPb collisions in the proton- and lead-going directions [6].

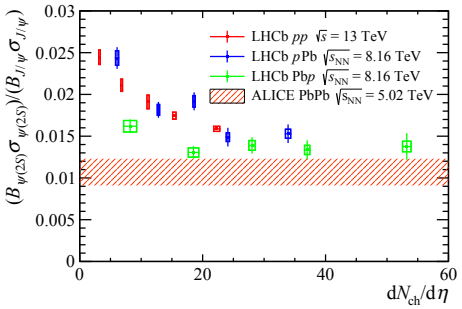

Figure 2. Ratio of production cross sections of $\psi(2S)$ to J/ψ mesons in pp and pPb collisions [8].

despite probing different initial-state configurations. These data constrain the impact of the initial state on flow-like signatures.

LHCb has also studied the multiplicity dependence of charmonium production in small collision systems. Charmonium suppression has been observed in high-multiplicity pp collisions by measuring the $J/\psi/\psi(2S)$ cross section ratio as a function of event multiplicity [7]. LHCb has now also measured this quantity in pPb collisions in both the proton- and lead-going directions [8]. The results are shown in Fig. 2. The lead-going results shown additional $\psi(2S)$ suppression relative to the pp and proton-going results, indicating additional sources of suppression in pPb collisions at backward rapidity.

3 Nucleon structure and low-x physics

LHCb's forward acceptance provides sensitivity to low-x partons in nuclei, reaching x less than 10^{-5}. Measurements of charm production in particular provide the strongest constraints on the gluon distribution in heavy nuclei [9]. LHCb has also studied the gluonic structure of nuclei using ultraperipheral PbPb collisions (UPCs). The detector's forward acceptance allows for the study of low-$p_{\rm T}$ particles, and the detector's hadron identification abilities are useful for studying low-mass hadronic resonances. LHCb is able to achieve clean samples of coherently produced ρ mesons, as shown in Fig. 3 [10].

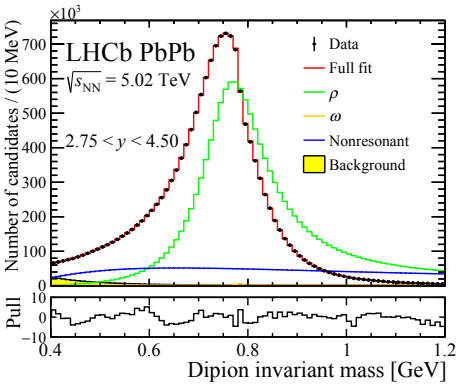

Figure 3. Dipion invariant mass distribution in UPCs showing ρ and ω signals [10].

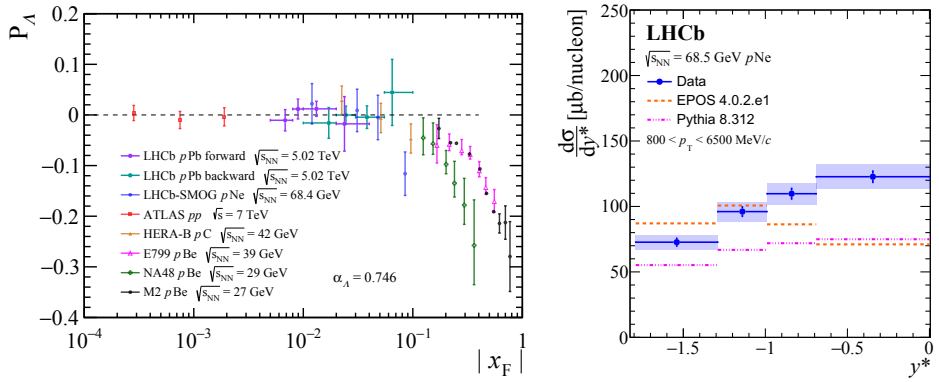

Figure 4. (Left) Transverse Λ polarization in pNe at $\sqrt{s_{NN}}$ = 68.5 GeV and pPb collisions at $\sqrt{s_{NN}}$ = 5.02 GeV compared to previous results [11, 12]. (Right) The ϕ meson cross section differential in center-of-mass rapidity in pNe collisions at $\sqrt{s_{NN}}$ = 68.5 GeV.

4 Fixed-target program

The SMOG gas injection system allows LHCb to function as a fixed-target experiment, covering central rapidity in the center-of-mass frame at energies around 100 GeV. This system has allowed LHCb to study a wide variety of collision systems. Between 2015 and 2018, LHCb collected fixed-target pNe, pHe, pAr, PbNe, and PbAr data. These data have been used to study particle production in a unique kinematic range. Fig. 4 (left) shows recent measurements of transverse Λ polarization using LHCb fixed-target and collider data [11, 12]. These data bridge the kinematic gap between older fixed-target experiments and recent collider measurements from the LHC. LHCb has also measured ϕ meson production in pNe collisions at $\sqrt{s_{NN}}$ = 68.5 GeV. Results are shown in Fig. 4 (right). These results disagree with predictions from Monte Carlo event generators, demonstrating that these data will be helpful for constraining event generators in unexplored kinematic regions.

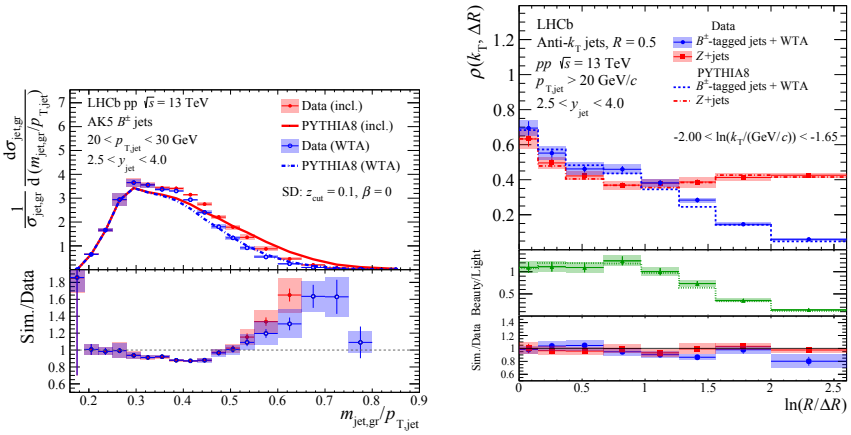

Figure 5. (Left) Groomed jet mass distribution for inclusive and WTA-tagged B jets. (Right) A projection of the LJP along the emission angle axis for light- and b-quark jets. Larger $R/\Delta R$ corresponds to smaller emission angles.

5 Jet physics

LHCb's vertexing and PID capabilities allow for precise studies of QCD emissions in heavy-flavor jets. Fig. 5 (left) shows the groomed jet mass distribution for jets tagged as heavy-flavor using fully-reconstructed B meson decays [14]. Two tagging algorithms are used: an inclusive algorithm that tags any jet containing a B meson as a heavy flavor jet, and a winner-take-all (WTA) algorithm, where the B meson is required to align with the WTA axis of the jet. The WTA axis is found by taking the direction of the highest-p_T subjet at each step of the jet reclustering. The use of different tagging algorithms allows for studying the QCD radiation pattern in heavy-flavor jets. QCD radiation can also be studied using the Lund Jet Plane (LJP). Fig. 5 (right) shows a LJP projection measured by LHCb for WTA B-tagged jets, as well as jets in $Z + j$ events which are predominantly produced by light quarks [15]. The projection is along the $R/\Delta R$ axis, where R is the jet radius parameter and $\Delta R = \sqrt{\Delta\phi^2 + \Delta\eta^2}$. Here $\Delta\phi$ and $\Delta\eta$ are the separation in azimuthal angle and pseudorapidity, respectively. The B-tagged jets show a suppression at small angles, consistent with the QCD dead cone effect and the first direct evidence for the dead cone effect in b jets.

6 LHCb in Run 3

The LHCb detector received a major upgrade before Run 3, which began in 2022 [16]. The tracking system was fully replaced, extending LHCb's reach in centrality from about 60% to about 30%. In addition, the front-end electronics were upgraded to read out the full detector at 40 MHz. LHCb uses this fast readout to process every collision in software using a GPU-based software trigger.

The SMOG system was also upgraded to SMOG2, a dedicated gas storage cell that can reach orders of magnitude higher pressure than the original SMOG system [17]. The dedicated gas cell also allows for clean separation between beam-beam and beam-gas collisions, allowing for simultaneous collider and fixed-target operation. As a result, SMOG2 is able to collect much larger samples than those collected by the original SMOG system. Fig. 6 shows

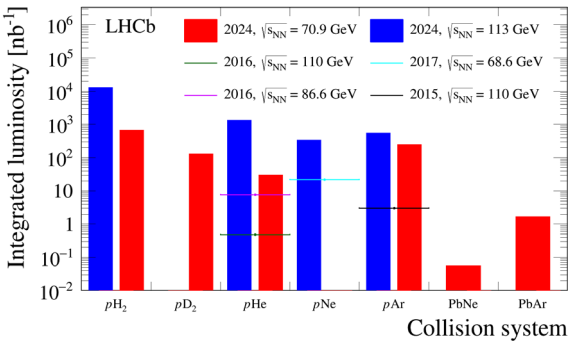

Figure 6. Integrated luminosities of beam-gas samples collected by LHCb in 2024. The recorded integrated luminosities are compared to those recorded in Run 2, which are shown by the horizontal bars.

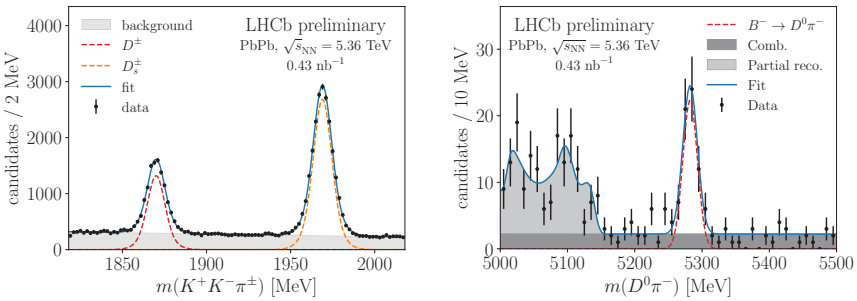

Figure 7. (Left)$D^\pm_{(s)}$ and (right) $B^\pm$ candidates from PbPb collisions at $\sqrt{s_{\rm NN}}$ = 5.36 TeV recorded by LHCb in 2024.

the integrated luminosities of the SMOG2 samples collected in 2024. These luminosities greatly exceed those collected in Run 2, in some cases by orders of magnitude.

LHCb collected its largest ever sample of PbPb data in 2024. Fig. 7 shows charm and bottom meson signals in PbPb collisions collected in 2024 [18]. The B meson signal is reconstructed in the $D^0(\to K^-\pi^+)\pi^-$ final state and is the first fully reconstructed, fully hadronic B meson decay in heavy ion collisions. The ability to reconstruct this decay model illustrates LHCb's potential to access previously unexplored heavy-flavor probes of heavy-ion collisions.

7 Conclusion

LHCb has a broad and growing heavy-ion physics program. The LHCb experiment recently collected unprecedented samples of PbPb collisions, as well as fixed-target pA and PbA collisions. These samples along with LHCb's acceptance and detector capabilities give LHCb a unique place in the high-energy nuclear physics landscape.

References

[1] A. A. Alves, Jr. *et al.* [LHCb], JINST **3**, S08005 (2008) doi:10.1088/1748-0221/3/08/S08005

[2] R. Aaij *et al.* [LHCb], Phys. Lett. B **762**, 473-483 (2016) doi:10.1016/j.physletb.2016.09.064 [arXiv:1512.00439 [nucl-ex]].

[3] S. Chatrchyan *et al.* [CMS], Phys. Lett. B **718**, 795-814 (2013) doi:10.1016/j.physletb.2012.11.025 [arXiv:1210.5482 [nucl-ex]].

[4] G. Aad *et al.* [ATLAS], Phys. Rev. Lett. **110**, no.18, 182302 (2013) doi:10.1103/PhysRevLett.110.182302 [arXiv:1212.5198 [hep-ex]].

[5] B. Abelev *et al.* [ALICE], Phys. Lett. B **719**, 29-41 (2013) doi:10.1016/j.physletb.2013.01.012 [arXiv:1212.2001 [nucl-ex]].

[6] R. Aaij *et al.* [LHCb], [arXiv:2505.09273 [nucl-ex]].

[7] R. Aaij *et al.* [LHCb], JHEP **05**, 243 (2024) doi:10.1007/JHEP05(2024)243 [arXiv:2312.15201 [hep-ex]].

[8] R. Aaij *et al.* [LHCb], [arXiv:2506.08624 [nucl-ex]].

[9] R. Aaij *et al.* [LHCb], Phys. Rev. Lett. **128**, no.14, 142004 (2022) doi:10.1103/PhysRevLett.128.142004 [arXiv:2108.13115 [hep-ex]].

[10] R. Aaij *et al.* [LHCb], [arXiv:2506.06250 [nucl-ex]].

[11] R. Aaij *et al.* [LHCb], JHEP **09**, 082 (2024) doi:10.1007/JHEP09(2024)082 [arXiv:2405.11324 [hep-ex]].

[12] R. Aaij *et al.* [LHCb], [arXiv:2508.02009 [nucl-ex]].

[13] R. Aaij *et al.* [LHCb], Eur. Phys. J. C **85**, no.5, 562 (2025) doi:10.1140/epjc/s10052-025-13852-4 [arXiv:2410.18018 [hep-ex]].

[14] R. Aaij *et al.* [LHCb], [arXiv:2505.11955 [hep-ex]].

[15] R. Aaij *et al.* [LHCb], [arXiv:2505.23530 [hep-ex]].

[16] R. Aaij *et al.* [LHCb], JINST **19**, no.05, P05065 (2024) doi:10.1088/1748-0221/19/05/P05065 [arXiv:2305.10515 [hep-ex]].

[17] O. Boente Garcia *et al.* Phys. Rev. Accel. Beams **27**, no.11, 111001 (2024) doi:10.1103/PhysRevAccelBeams.27.111001 [arXiv:2407.14200 [physics.ins-det]].

[18] R. Aaij *et al.* [LHCb], LHCb-FIGURE-2025-004